H NMR Metabolomics analysis of renal cell carcinoma cells: Effect of VHL inactivation on metabolism

Cuperlovic-Culf, Miroslava; Cormier, Kevin; Touaibia, Mohamed; Reyjal, Julie; Robichaud, Sarah; Belbraouet, Mehdi; Turcotte, Sandra

Publisher's version / Version de l'éditeur:
https://doi.org/10.1002/ijc.29947
International Journal of Cancer, 2015-11

^{1}H NMR Metabolomics analysis of renal cell carcinoma cells: Effect of VHL inactivation on metabolism

Miroslava Cuperlovic-Culf[1,2*], Kevin Cormier[2], Mohamed Touaibia[2], Julie Reyjal[2], Sarah Robichaud[2], Mehdi Belbraouet[2], Sandra Turcotte[2,3*]

[1] National Research Council of Canada, 100 Rue des Aboiteaux St.; Moncton, NB E1A 7R1, Canada

[2] Department of Chemistry and Biochemistry, Université de Moncton, Moncton, NB E1A 3E9, Canada

[3] Atlantic Cancer Research Institute, Moncton, NB E1C 8X3, Canada

To whom correspondence should be addressed: Miroslava Cuperlovic-Culf, National Research Council of Canada, 100 Rue des Aboiteaux St.; Moncton, NB E1A 7R1, Canada, Tel.: (506) 861-0952; E-mail: miroslava.cuperlovic-culf@nrc-cnrc.gc.ca.

Abstract

Von Hippel-Lindau (*VHL*) is an onco-suppressor involved in oxygen and energy-dependent promotion of protein ubiquitination and proteosomal degradation. Loss of function mutations of *VHL* (VHL- cells) result in organ specific cancers with the best studied example in renal cell carcinomas. VHL has a well-established role in deactivation of hypoxia-inducible factor (HIF-1) and in regulation of PI3K/AKT/mTOR activity. Cell culture metabolomics analysis was utilized to determined effect of VHL and HIF-1α or HIF-2α on metabolism of renal cell carcinomas (RCC). RCC cells were stably transfected with *VHL* or shRNA designed to silence *HIF-1α* or *HIF-2α* genes. Obtained metabolic data was analysed qualitatively, searching for overall effects on metabolism as well as quantitatively, using methods developed in our group in order to determine specific metabolic changes. Analysis of the effect of *VHL* and *HIF* silencing on cellular metabolic footprints and fingerprints provided information about the metabolic pathways affected by VHL through HIF function as well as independently of HIF. Through correlation network analysis as well as statistical analysis of significant metabolic changes we have determined effects of VHL and HIF on energy production, amino acid metabolism, choline metabolism as well as cell regulation and signaling. VHL was shown to influence cellular metabolism through its effect on HIF proteins as well as by affecting activity of other factors.

Keywords: NMR Metabolomics; renal cancer; RCC; VHL; hypoxia; HIF; cancer metabolism

Novelty and Impact

Mutation in *VHL* gene is the major characteristic of renal cell carcinomas affecting metabolism of these cells through VHL's effect on function of HIF and through other factors. NMR metabolomics analysis provided information about specific VHL and HIF effects on renal cell carcinomas metabolism. Metabolic changes induced by cancer-driving gene mutations provide avenue for development of novel biomarkers and therapies.

Introduction

Kidney cancer is amongst top 10 most common malignancies in both genders (1). Renal cell carcinoma (RCC) accounts for nearly 90% of all kidney cancers (2, 3). Although several different risk factors of RCC have been explored, mutation in von Hippel-Lindau (VHL) is a ubiquitous genetic predisposition for the development of RCC (4). In fact 70-90% of clear cells RCCs demonstrate mutation or gene silencing of *VHL* (5, 6). It has been previously shown that VHL-deficient cells could be targeted using specific small molecules. This approach based on synthetic lethality shows is highly advantageous as it targets kidney cancer cells while sparing normal tissue (7, 8). RCCs, largely due to the mutation in *VHL*, show number of unique characteristics including highly distinct expression of enzymes as well as number of different metabolic features when compared to either normal kidney cells or other tumours (9). Transformation of cellular metabolism is a necessary step in the development of RCCs that correlates with tumour stage and severity. Apart from the significance specifically to renal cancers, *VHL*-mutation induced metabolism changes make RCCs an excellent model for the analysis of oncogenic metabolic shift.

Number of gene expression changes have been observed and related to the unique metabolism of RCC. Briefly, RCC samples show strong down-regulation of genes involved in tricarboxylic acid (TCA) cycle as well as AMP-activated protein kinase (AMPK) and phosphatidylinositol 3,4,5-trisphosphate 3-phosphatase (PTEN). At the same time genes involved in the pentose phosphate pathway (PPP) are up-regulated in RCC samples. Finally, glutamine transporter genes as well as acetyl-CoA carboxylase protein show increased activity in these cells (10). Loss of function of *VHL* gene as well as inhibition of fructose-1,6-bisphosphatase 1 (FBP1), which is a rate-limiting gluconeogenic enzyme, are major factors related to genetic and metabolic changes observed in RCC cancer patients (11). Germline or somatic mutations in *VHL* have been indicates as factors in the development of several highly vascularized tumours including clear-cell type of renal cell carcinoma (RCC) as well as some subtypes of pancreatic cancer. VHL has a major role as an E3 ubiquitin ligase that negatively regulates the hypoxia inducible factor (HIF) in normal conditions (12). Under normoxic conditions, HIF-α is prolyl-hydroxylated, through the action of prolyl-hydroxylase domain proteins (PHDs). This form of HIF-α is recognized and degraded by VHL. Under hypoxic conditions PHDs are inactive and HIF-α is stabilized regardless of VHL function. The complex formed by HIF-α and the constitutively expressed HIF-1β binds to the hypoxia-response element (HRE) of several genes for transactivation. Two isoforms of HIF-α – HIF-1α and HIF-2α – (13) have highly similar structures and both are degraded by VHL under normoxic conditions. However, despite very similar sequences, HIF-1α is ubiquitously expressed while HIF-2α is limited to endothelium, kidney, heart, lungs and small intestine (14). Although HIF-1α and HIF-2α can activate the same target genes, they also show specificity. HIF-1α activates glycolytic enzyme genes and HIF-2α targets preferentially vascular endothelium growth factor (VEGF), transforming growth factor-α (TGFα), lysyl oxidase and cyclin D1. In addition, they show different functions in tumor development with HIF-2α and not HIF-1α promoting tumor growth in RCC (15, 16).

Relationship between FBP1 and metabolism of RCC cells, specifically glycolysis and PPP have been studied recently (11). In *VHL* deficient cells, FBP1 restrains cell proliferation, glycolysis and PPP by inhibiting transcription functions of HIF. Therefore absence of FBP1 is a necessary prerequisite for the development of unique, HIF-driven metabolism of VHL-deficient cells.

HIF has a major effect on cell metabolism through several transcription functions. HIF regulates expression of glucose transporters and, in VHL-deficient RCC cells, glucose transporter 1 (GLUT1) is overexpressed (1, 17-19). HIF also up-regulates transcription of number of glycolysis pathway enzymes including hexokinase 1 and 2 (*HK1* and *HK2*) and glyceraldehyde 3-phosphate dehydrogenase (*GADPH*). Furthermore, lactate dehydrogenase (*LDH*) and pyruvate dehydrogenase kinase 1 (*PDK1*) are up-regulated by HIF. LDH promotes conversion of pyruvate from glycolysis into lactate leading to generation of NAD+ from NADH. PDK1 inhibits function of pyruvate dehydogenase (PDH) effectively blocking transfer of pyruvate into mitochondria and its conversion into acetyl CoA. In this way mutation

of VHL followed by activation of HIF up-regulate glycolysis and divert TCA cycle away from glucose as a preferred fuel.

In addition to HIF1 and HIF2, VHL affects expression of number of other genes with 30 targets identified in *VHL* transfected RCC cells (20). These include number of metabolite transporters and enzymes including for example glutaminase, major enzyme involved in generation of glutamate from glutamine and monocarboxylate transporter – carrier of monocarboxylates (e.g. lactate and pyruvate) across biological membrane. VHL also regulates expression of insulin-like growth factor receptor (IGF1R) in an HIF independent manner. IGF1R regulates phosphoinositide-3-kinase (PI3K), which in turn activates AKT signalling and regulates signalling by mammalian target of rapamycin (mTOR) (21). mTOR is key regulator of cellular metabolism serving as a nutrient sensor and one of the regulators of protein, nucleotide and lipid synthesis aimed at promoting cell growth (for recent review see 22). mTOR activates pyrimidine synthesis and pentose phosphate pathways, lipogenesis and ribosome biogenesis. It is also involved in the regulation of amino acid levels and utilization.

Detailed gene expression analysis of Gatto and co-workers (9) showed major remodelling of metabolic genes in RCC cells when compared to normal as well as other cancer cells. They established that the loss of heterozygosity in several major metabolic genes that are adjacent to *VHL* compromise nucleotide, one-carbon, inositol metabolism and glycerolipid biosynthesis. This effect leads to the loss of redundancy as well as down-regulation of several metabolic processes such as for example metabolism of branched chain amino acids. At the same time, genes involved in glycine synthesize from choline via betaine and dimethylglycine are overexpressed in RCC cells suggesting increased significance for this pathway in VHL mutant cells (9).

In this work we have set out to determine the effects of VHL, HIF-1α and HIF-2α proteins on metabolic profile of Kidney cancer, RCC, cells. Metabolomics can provide complementary information to the previously published gene expression analysis. Unlike genomics and transcriptomics that show only possibility for cellular activity, metabolomics measures outcomes of functional metabolic pathways. Thus, metabolomics provides data for testing of genomics-driven hypothesize about cell behaviour and changes. In order to observe effects of VHL through its effect on HIF and independently of HIF we have explored metabolic changes in kidney cell lines following *VHL* transfection, leading to deletion of both HIF-1α and HIF-2α, as well as metabolic changes induced by silencing of either *HIF-1α* or *HIF-2α* in VHL$^-$ cells. NMR metabolomics methodology previously developed in our group for the analysis of mammalian cell cultures (23) was used in this work.

Material and Methods

Cell culture procedures: Human RCC10 cells negative for *VHL* and RCC with *VHL*-reintroduced (RCC10/*VHL*) were kindly provided by Amato Giaccia (Stanford University, Stanford, CA). Cells were maintained in DMEM high glucose supplemented with L-glutamine and 10% FCS. Authentication of VHL-expressing and negative (parental) cells was performed by short tandem repeat (STR) DNA profile at Genetica DNA Laboratories (Burlington, NC, USA). All experiments were performed as five independent replicates (5 biological replicates). Cell harvesting was performed 48h and 72h post treatment. Intracellular, hydrophilic metabolite isolation was performed as described previously (23, 24, 25). Cells were harvested by scraping and rinsed with 5 mL of PBS. The mixture was centrifuged at 4000 RPM for 1 min. The supernatant was discarded and the cell pellet was rinsed with 4 mL of PBS. Following another centrifugation at 4,000 RPM for 1 min, the cell pellets were kept on ice for 5 min before being re-suspended in 1 mL of ice-cold acetonitrile/water (1:1). Cell suspensions were kept on ice for 10 min before centrifugation at 16,000 RPM for 10 min at 4 °C. The aqueous acetonitrile extract supernatants were dried under a stream of N2. To isolate extracellular metabolites, 500 µL of extracellular medium were pipetted from cells. The samples were subsequently centrifuged at 200 RCF for 5 min. The supernatant was used as the extracellular fraction.

Stable transfection for HIF-1α and HIF-2α knockdown: To stably decrease *HIF-1α* or *HIF-2α*, RCC10 cells were transduced with pLKO.1 lentivirus expressing shRNA constructs for *HIF-1α* (TRCN0000003808 and 3810) and *HIF-2α* (TRCN0000003804 and 3807) from Open Biosystem. Briefly,

lentivirus were produced by co-transfecting the plasmid sequence and the lentiviral packaging mix in the 293FT cells. The supernatant was collected after 48h and 72h and concentrated by ultracentrifugation. RCC10 cells were used for infection in presence of 6μg/mL polybrene. Media were changed 16-20 hrs after infection and transduced cells were selected with puromycin. Cells were tested for HIF-1α and HIF-2α protein expression by western blot analysis and mRNA *HIF* targets by qRT-PCR.

NMR experimentation: The hydrophilic metabolites obtained after drying were dissolved in 0.7 mL of deuterium oxide (Aldrich, 99.96 atom% 2H) and pipetted into a 5mm NMR tube for NMR analysis. To the extracellular metabolites (0.5 mL) 0.2 mL of deuterium oxide (Aldrich, 99.96 atom% 2H) was added prior to transfer into 5mm NMR tube. All ^{1}H NMR measurements were performed on a Bruker Avance III 400 MHz spectrometer at 298K. 1D spectra for hydrophilic and extracellular samples were obtained using a gradient water presaturation method (26) with 512 scans. Standard parameters were used with gradient duration of 1ms and recovery delay after the gradient of 100μs. NMR spectra were processed using Mnova with exponential apodization; global phase correction; Berstein-Polynomial baseline correction; Savitzky-Goley line smoothing and normalization using total spectral area as provided in Mnova. Spectral regions from 0.5-4.5 ppm and 5-9 ppm were included in the normalization and analysis.

Data analysis: Data pre-processing including data organization, removal of undesired areas, normalization, as well as data presentation was performed with Matlab vR2010b (Mathworks). Minor adjustments in peak positions (alignment) between different samples were performed using in-house developed alignment software (http://gast.nrcbioinformatics.ca) as well as a publicly available method Icoshift for automatic spectral alignment (27). Principal component analysis (PCA) was done using the Matlab platform and hierarchical clustering was performed with TMeV software. Correlation analysis and network presentation was performed using Matlab. Feature selection was done with the Significance analysis for microarrays (SAM) method (28) as provided in TMeV. Peak assignment was performed using several methods developed in our group and elsewhere and was based on metabolic NMR databases (www.hmdb.ca and www.bmrb.wisc.edu). Spectra for 30 metabolite in extracellular and 38 for intracellular medium used in quantification were obtained from the Human Metabolomics Database (www.hmdb.ca) or Biological Magnetic Resonance Databank (www.bmrb.wisc.edu) and further analyzed visually and compared to the obtained spectra.

Metabolite quantification: An automated method for quantification based on multivariable linear regression of spectra with appropriately aligned standard metabolite data from databases was developed previously (23) and utilized in this study. The assumption behind this approach is that the spectrum of a mixture is the same as the combination (sum) of spectra of individual components measured under the same conditions. Here relative metabolite concentrations were estimated using nonlinear curve-fitting with the multivariate least-squares approach. The partial least squares regression analysis result was used as the starting point and the model was constrained to concentrations greater than or equal to zero. The deconvolution of spectra of mixtures, such as in metabolomics, with many strongly overlapping lines, possibly with an unknown number of lines and atomic groups, each with a different line width is extremely difficult and thus it is important to determine an optimal solver for this problem. Generally, the solution is found by minimizing the square root of difference between the model and the real spectrum. The best result, *i.e.* the model with a minimal error was obtained with Levenberg-Marquardt curve fitting and this method was used for quantification of metabolic data used in further analysis. The Levenberg-Marquardt method is specifically designed for solving non-linear curve-fitting problems in a least-squares sense and additionally allows inclusion of a constraint that concentrations have to be non-negative. Quantification error is estimated by performing the multivariate linear regression analysis as described above but with one metabolite at a time removed from the analysis. In this way, we are estimating errors caused by omitting metabolites from the analysis and the uniqueness of spectral features for metabolite quantification. Values for metabolite concentrations and the errors can be obtained by request from the authors.

Results and discussion

NMR metabolomics analysis was performed on *VHL*-deficient wild type RCC10 cells (VHL^-), on RCC10 cells transfected with *VHL* (VHL^+), RCC10 VHL^- cells treated with small hairpin RNA (*shRNA*) silencing *HIF-1α* (shHIF1) and *HIF-2α* (shHIF2). Silencing of *HIF-1α* and *HIF-2α* was done with two different *shRNA* sequences for comparison. Protein levels of HIF-1α and HIF-2α in these cells are shown in Figure 1A and groups of samples are schematically outlined in Figure 1B. Western blot analysis of protein levels shows agreement with expected effects of VHL transfection as well as HIF protein silencing. In addition, BNIP3 and VEGFA mRNA levels were quantified and showed significant downregulation in HIF-1α and HIF-2α knockdowns, respectively (Figure 1C).

FIGURE 1. AROUND HERE

Cell line RCC10 lacks functional pVHL due to a mutation in the VHL gene. In the absence of VHL, RCC10 cells express both HIF-1α and HIF-2α (29) and this effect is clearly visible in Figure 1A, column RCC10. Transfection of VHL leads to deletion of both HIF-1α and HIF-2α (VHL^+). It is evident from Western Blots that specific silencing of HIF-1α and HIF-2α can be achieved with used sequences (shRNA sequence information is provided in Material and Methods) leading to complete deletion of HIF-1α and no effect on HIF-2α (shHIF1) or complete deletion of HIF2 and no effect of HIF1 (shHIF2). For quick reference the presence of VHL, HIF-1α and HIF-2α in four cell groups is schematically shown in Figure 1B. This grouping will be used for further analysis.

Hydrophilic intracellular and extracellular metabolic extracts were obtained from five biological replicates of each sample type. Sampling of control (VHL^-) and VHL^+ cells was performed after 48h and 72h in cell cultures. Samples of cells treated with shHIF1 and shHIF2 were collected after 72h in the culture. ^{1}H NMR spectra were measured for hydrophilic metabolites from intracellular (fingerprint) and extracellular medium (footprint). Metabolic analysis was performed qualitatively, directly on the NMR spectra and quantitatively, on metabolite concentrations obtained from the NMR spectra using method presented elsewhere (23). NMR spectra and quantified metabolic data of all groups of samples studied is shown in Supplementary Data (Supp. Figure 1). Both NMR spectra and quantified metabolic data are available from the authors.

PCA of spectra for VHL^- and VHL^+ cells at 48h and 72h in cultures (Figure 2) shows clear separation by VHL status as well as the time in the culture in spectra and relative concentrations of intracellular and extracellular metabolites. It is apparent from both spectral as well as the metabolite concentrations investigation that transfection of *VHL* in RCC10 cell lines induces large metabolic shift which increases with time spend in cell culture (Figure 2).

FIGURE 2. AROUND HERE

According to PCA, *VHL* transfection causes larger change in metabolic profile of extracellular than intracellular media. In both cases VHL^- and VHL^+ samples are separated on principle component 1 (PC1), however in intracellular medium, PC1 represents 53% of variance in the data while for extracellular metabolites 74% of data variance is represented by PC1. We have observed similar trend in metabolomics analysis of drug treated cells (25) possibly due to cells self-preservation at the expense of changes in extracellular environment. In addition, number of small molecule transporters is down-regulated in VHL^- tumours (11) and their re-establishment with *VHL* transfection can lead to large changes in extracellular metabolic status. However, intracellular metabolic shift over time is larger than for extracellular metabolites (with PC2 of over 23% relative to 19% in extracellular media analysis) suggesting a significant accumulation of metabolic changes induced by *VHL* transfection.

Quantified metabolic data from cells obtained at two time points was used to determine correlations between metabolites in VHL^- and VHL^+ state. Boxplot analysis of metabolic data shows skewness suggesting a non-normal distribution (not shown). In addition, concentration levels do not have to be linearly related. Therefore, Spearman correlation analysis was used. It should be mentioned however that highly comparable results were obtained using Pearson correlation calculation. Comparison between Spearman correlation values of metabolites in VHL^- and VHL^+ cells in intracellular and extracellular

media are shown in Supplementary Figure 2. Different correlation levels between metabolites in the presence and absence of VHL are apparent. For easier visualisation Spearman correlations are presented as a network between metabolites (Figure 3). Only correlation coefficients over 0.85 are shown as connections in the network.

FIGURE 3. AROUND HERE

Analysis of metabolic changes in intracellular medium of VHL^- cells (Figure 3A) shows close correlation between glutamine and number of metabolites including amino acids, TCA cycle intermediates and glutathione (GSH). Direct, strong correlation between glutamine, glutamate, citrate suggests that VHL^- cells utilize glutamine for citrate production in TCA cycle in agreement with previous report that hypoxic and VHL^- use glutamine to generate citrate and lipids through carboxylation of oxoglutarate (13). Analysis of VHL^- cells' extracellular medium (Figure 3C) further indicates correlation between glutamine and lactic acid. Interestingly, in VHL^- cells glucose is strongly correlated only with amino acids – taurine intracellularly and others extracellularly. Previous work has shown the incorporation of glucose into amino acids including taurine in cancers (30) and according to the results shown here this is driven by the VHL possibly through the effect on HIF functions. Major correlation between glucose and amino acids in VHL^- cells speaks to its utilization for biomolecule production instead of fueling TCA cycle.

In VHL^+ cells glucose concentration change is once again correlated with taurine but this time also glutamate, several TCA intermediates, choline and GSH indicating utilization of glucose for TCA cycle in these cells. Concentration changes in glutamine is in VHL^+ cells correlated only with amino acids and extracellular glutamine concentration changes are not strongly correlated with any of the measured metabolites, once again suggesting reduced utilization of glutamine in VHL^+ cells.

Significance Analysis of Microarray (SAM) was used to determine significantly differentially concentrated metabolites in relation to the levels of VHL, HIF-1α and HIF-2α. Metabolites that are significantly differentially concentrated in VHL^- and VHL^+ cells are shown in Supplementary Figure 3. These include linear and branch chain amino acids, metabolites involved in glycolysis and TCA cycle and choline derivatives. In VHL^- cells glucose utilization is increased with reduced intra- and extracellular concentration of glucose however it is largely used for production of lactate with observed increase in lactate concentration intra- and extracellularly (Figure 3). In VHL^+ cells glucose concentration changes become more strongly correlated with amino acids and also TCA cycle intermediates and choline, suggesting that glucose is used as a main carbon source in these cells (Figure 3 B and D). Transfection with *VHL* changes cells metabolism of amino acids including transport and metabolism of branched chain amino acids (Figure 4). Valine and Isoleucine are significantly less utilized in VHL^- cells with clear up-concentration in both intra- and extra-cellular medium (Figures 3 and 6). Similar behaviour is observed for asparagine, threonine, and alanine. These results are in agreement with information resulting from gene expression analysis showing that metabolism of alanine, aspartate and glutamate was less altered in RCCs than in other cancers (9). Enzymes involved in metabolism of amino acids (valine, leucine, isoleucine, cysteine, methionine, glycine, serine and threonine), TCA cycle, metabolism of ubiquinone and ubiquinol and electron transport chain were also significantly downregulated in RCC cells when compared to normal renal cells as well as cells of other cancer types (9).

Concentration of glutamate and histidine is lower in intracellular medium of VHL^- than VHL+ cells, however their concentration is higher in extracellular medium of VHL- cells. Thus, glutamine transport into cells appears increased in VHL^- cells (Figure 4) in agreement with previous work (10) . Glutamine concentration change in VHL^- cells is highly correlated to the concentration changes of number of other metabolites including amino acids, citrate, lactic acid production (Figure 3, A and C). Reduced concentration of glutamate in the intracellular medium of VHL^- cells could be in part due to its increased use as fuel for TCA cycle. At the same time glutamate in the extracellular medium in VHL^- cells shows significantly higher concentration when compared to VHL^+ cells. Similar effect has been observed in MB-231, breast cancer cell lines in hypoxic conditions (31). Glutamate is an immunosuppressive metabolite that is often released by the cells as a protector against immune systems

attack (32, 33). Increase of extracellular glutamate in hypoxic cells as well as VHL$^-$ cells suggests a relationship with HIF factor function. This observation is in agreement with recent work of Hu et al. (34) showing HIF-dependent expression of glutamate transports SLC1A and SLC1A3.

FIGURE 4. AROUND HERE

Malate is produced by TCA cycle in mitochondria and when exported into cytoplasm can be used for production of pyruvate and lactate leading to generation of NADPH. NADPH is a major energy source in citrate-driven fatty acid synthesis. L-alanine has significantly higher concentration in both extra- and intracellular media of VHL$^-$ cells in comparison to VHL+ cells. L-alanine can be produced from pyruvate coupled to the catabolism of branch chain amino acids in presence and conversion of glutamate to oxoglutarate. With observed increase in concentration of both L-alanine and oxoglutarate and reduced concentration of glutamate in VHL$^-$ cells, role of pyruvate should be further investigated.

VHL$^-$ cells show low levels of choline but high level of serine with opposite effect in VHL$^+$ cells. This could be, at least in part, due to choline degradation to glycine, process which is up-regulated in high-stage RCC, VHL$^-$ tumours (9).

Myoinositol has significantly lower concentration in VHL$^-$ relative to VHL+ cells, once again in agreement with the observation that genes involved in inositol metabolism in VHL$^-$ cells are downregulated or missing (9). Transfection of *VHL* to RCC cells possibly increases expression of inositol metabolism genes as suggested by the major increase in myoinositol level observed in VHL$^+$ cells.

Extracellular levels of adenosine are significantly increased in VHL$^-$ cells. Extracellular adenosine has been shown to accumulate under conditions of cellular metabolic stress and hypoxia (35, for review see 36). Accumulation of extracellular adenosine induces apoptosis in various cancer cells and its effect on VHL$^-$ cells has been previously outlined (37).

Metabolic changes resulting from *VHL* transfection are result of either loss of HIF-1α, HIF-2α or other proteins affected by VHL. In order to investigate specific HIF-1α or HIF-2α induced metabolic changes as well as non-HIF-α related VHL effects we have explored changes in metabolic profiles of RCC10 VHL$^-$ and VHL$^+$ cells in comparison to VHL$^-$ cells with *HIF-1α* or *HIF-2α* genes silenced. According to the PCA of spectral data (Supplementary Figure 3) the effect of *VHL* transfection on metabolism of RCC10 cells is larger than the individual effects of HIF-1α and HIF-2α. Large separation in PC1 is observed between VHL$^-$ and VHL$^+$ cell samples in both intracellular and extracellular medium (PC1 equals 76% and 90% respectively). But, silencing of *HIF-1α* or *HIF-2α* also leads to observable metabolic changes. Supplementary Figure 3B shows comparison between intra- and extracellular metabolic profiles of VHL$^-$ cells and VHL$^-$ cells treated with either *HIF-1α* or *HIF-2α* silencing sequences. In this group the largest metabolic change, according to PCA, is induced by silencing of *HIF-1α*. This group shows the effect of only HIF-1α or HIF-2α as neither group of cells contains functional VHL protein. Comparison between VHL$^+$ cells and VHL$^-$ cells with silenced *HIF-1α* or *HIF-2α* is shown in Supplementary Figure 3C. Not surprisingly, metabolic changes observed in this group are much larger then in Supplementary Figure 3B as they show changes in metabolic profiles due to gain of function of VHL (leading to loss of function of HIF-1α and HIF-2α) and functional HIF-1α or HIF-2α. Specific alterations in metabolite concentrations that can be ascribed to each of these groups are determined using SAM method for feature selection (Figure 5 and 6). Figure 5 shows metabolic differences between cells with or without HIF-1α or cells with either VHL or with HIF-1α function. Figure 6 shows metabolic changes that can be ascribed to change in HIF-2α or VHL and HIF-2α function.

Silencing of *HIF-1α* gene in VHL$^-$ cells only induces to some of the metabolic effects observed in transfection of *VHL* (Figure 6). According to metabolic measurements presented here, HIF-1α causes increase in glucose import and utilization, production of lactic acid, increased release of glutamate as well as number of changes to TCA cycle intermediates and amino acids. Change in only HIF-2α activity (Figure 6) induces some of the same effects and HIF-1α including glucose utilization and glutamate and lactic acid production.

FIGURE 5. AROUND HERE

FIGURE 6. AROUND HERE

Taurine levels in extracellular medium are significantly increased in VHL^+ compared to VHL^- cells as well as shHIF-1α cells compared to VHL^- cells and VHL^+ cells when compared to shHIF-1α or shHIF-2α cells. This suggests a role of HIF-1α and HIF-2α in reducing transport of taurine out of the cell. Taurine is an important osmo- and volume regulator in cells. Hypotaurine acts as an antioxidant and can possibly protect cells from free-radical damage. Concentration of taurine has been shown to increase in $HIF\text{-}2^+$ tumours (38).

Supplementary Figure 4 and 5 demonstrate relative concentration changes, intracellularly (top row in the color table) and extracellularly (bottom row in the color table), for significantly affected metabolites in different groups of samples. Supplementary Figure 4 shows the effect of change in VHL and HIF-1α and HIF-2α function together (first column showing comparison between VHL^- and VHL^+ samples) compared to effects of change in HIF-1α (second column showing comparison between VHL^- and shHIF-1α samples) or HIF-2α (third column showing comparison between VHL^- and shHIF-2α samples). Supplementary Figure 5 shows in all three cases change in VHL where first column shows change in VHL and HIF-1α and HIF-2α (showing comparison between VHL^- and VHL^+ samples), second column shows the effect of change in HIF-2α and VHL status (showing comparison between VHL^+ and shHIF-1α samples), and third column shows the effect of change in HIF-1α and VHL function (showing comparison between VHL^+ and shHIF-2α samples). Functionality of VHL, HIF-1α and HIF-2α for each sample group studied and presented in Supplementary Figure 4 and 5 are provided in the table within the figure. Several things are apparent from this representation. First, expression of either HIF-1α or HIF-2α is sufficient for increased glucose utilization from the medium and within the cells leading to increased lactate production. Also, increase in extracellular glutamate is significant with either functional HIF-1α or HIF-2α. Several metabolic changes are significant only with the change in VHL and one of the HIF proteins. These include increased concentration of choline and phosphocholine (PC) with functional VHL. Both intracellular and extracellular choline concentrations are increased in VHL^+ cells regardless of HIF status. Although HIF expression increases choline and PC levels, in agreement with previous studies (39), transfection of these cells with *VHL* leads to further increase. Best to our knowledge this effect of *VHL* on choline metabolites has not been previously observed and requires further exploration. Intracellular glutamate is significantly increased in the presence of functional VHL but not significantly affected by HIF-1α or HIF-2α. At the same time, extracellular glutamine has higher concentration in the extracellular medium of VHL^+ cells, therefore suggesting another avenue for glutamate production in these cells.

Conclusions

Metabolism of renal cancer cells is significantly different from normal renal cells as well as other cancers. Specific metabolic characteristics are the result of loss of functional *VHL* gene and activation of hypoxic response with active HIF-1α and HIF-2α genes. In this work, we have shown that *HIF-1α* and *HIF-2α* genes lead to increased glycolysis, altered TCA cycle and increased production of extracellular glutamate amongst other effects. VHL on the other hand has a major effect on choline metabolism as well as metabolism of amino acids. Observed metabolic changes can suggest clinical biomarkers for VHL^- tumours as well as $HIF\text{-}2\alpha^+$ and $HIF\text{-}2\alpha^+$ tumours. In addition, specific properties of choline and amino acids metabolism in VHL^- cells might lead to interesting targets for future investigation.

Acknowledgments: The authors would like to thank Monique Monette, Julien Dong and Robin Stein (Bruker Canada) for their help in setting up the NMR experiments. Mohamed Touaibia acknowledges the contribution of the Canadian Foundation for Innovation (CFI), the New Brunswick Innovation Foundation (NBIF) and Université de Moncton. Mohamed Touaibia would also like to acknowledge the support of the CFI for the funding of a portion of the operating costs and maintenance for the NMR instrument through the Infrastructure Operating Fund (IOF). Miroslava Cuperlovic-Culf

would like to acknowledge support from National Research Council for software tools used in data analysis. A KRESCENT New Investigator award sponsored Sandra Turcotte. This study was supported in part by NBHRF, NBIF and CIHR grants from Sandra Turcotte.

References

1. Sudarshan, S., Karam, J., Brugarolas, J., Thompson, R. H., Uzzo, R., Rini, B., Margulis, V., Patard, J.J., Escudier, B., Linehan, W.M. (2013). Metabolism of kidney cancer: from the lab to clinical practice. *European Urology*, **63**: 244–51.
2. Ljungberg, B., Cowan, N.C., Hanbury, D.C., Hora, M., Kuczyk, M.A., Merseburger, A.S., Patard, J.J., Mulders, P.F., Sinescu, I.C. European Association of Urology Guideline Group. (2010). EAU guidelines on renal cell carcinoma: the 2010 update. *Eur Urol.* **58**: 398-406.
3. Monteiro, M. S., Carvalho, M., de Lourdes Bastos, M., and de Pinho, P. G. (2014). Biomarkers in renal cell carcinoma: a metabolomics approach. *Metabolomics*, **10**: 1210–1222.
4. Gerlinger M, Horswell S, Larkin J, Rowan AJ, Salm MP, Varela I, Fisher R, McGranahan N, Matthews N, Santos CR, Martinez P, Phillimore B, Begum S, Rabinowitz A, Spencer-Dene B, Gulati S, Bates PA, Stamp G, Pickering L, Gore M, Nicol DL, Hazell S, Futreal PA, Stewart A, Swanton C. Genomic architecture and evolution of clear cell renal cell carcinomas defined by multiregion sequencing, (2014) *Nature Genetics,* **46**: 225-233.
5. Kim, W.Y., Kaelin, W.G. (2004) Role of VHL gene mutation in human cancer. *J Clin Oncol*; **22**:4991–5004.
6. Moore, L.E,. Nickerson, M.L., Brennan, P., et al. (2011) Von Hippel-Lindau (VHL) inactivation in sporadic clear cell renal cancer: associations with germline VHL polymorphisms and etiologic risk factors. *PLoS Genet*. **7**:e1002312.
7. Turcotte S, Chan DA, Sutphin PD, Hay MP, Denny WA and Giaccia AJ. A molecule targeting VHL-deficient Renal Cell Carcinoma that induces autophagy. (2008) *Cancer Cell* **14**: 90-102.
8. Chan DA, Sutphin PD, Nguyen P, Turcotte S, Lai EL, Wu J, Solow-Cordero DE, Bouley DM, Graves EE, Denny WA, Hay MP, Giaccia AJ. Targeting Glut1 and the Warburg Effect in Renal Cell Carcinoma by Chemical Synthetic Lethality. (2011) *Sci. Transl. Medicine* **3**(94):94ra70.
9. Gatto, F., Nookaew, I., and Nielsen, J. (2014). Chromosome 3p loss of heterozygosity is associated with a unique metabolic network in clear cell renal carcinoma. *Proc National Acad Sci*, 111: E866–75.
10. CGARN: The Cancer Genome Atlas Research Network (2013). Comprehensive molecular characterization of clear cell renal cell carcinoma. *Nature*, **499**: 43–9.
11. Li, B., Qiu, B., Lee, D.S.M., Walton, Z.E., Ochocki, J.D., Mathew, L.K., Mancuso, A., Gade, T.P., Keith, B., Nissim, I., Simon, M.C. (2014). Fructose-1,6-bisphosphatase opposes renal carcinoma progression. *Nature*. **513**: 251-255.
12. Bader, H. L., and Hsu, T. (2012). Systemic VHL gene functions and the VHL disease. *FEBS letters*, **586**: 1562–1569.
13. Gameiro, P., Yang, J., Metelo, A. M., Pérez-Carro, R., Baker, R., Wang, Z., Arreola, A., Rathmell, W.K., Olumi, A., López-Larrubia, P., Stephanopoulos, G., Iliopoulos, O. (2013). In vivo HIF-mediated reductive carboxylation is regulated by citrate levels and sensitizes VHL-deficient cells to glutamine deprivation. *Cell Metabolism*, **17**: 372–85.
14. Wiesener, M.S., Jurgensen, J.S., Rosenberger, C., Scholze, C.K., Horstrup, J.H., Warnecke, C., Mandriota, S., Bechmann, I., Frei, U.A., Pugh, C.W., Ratcliffe, P.J., Bachmann, S., Maxwell, P.H., Eckardt, K.U.. (2003) Widespread hypoxia-inducible expression of HIF-2alpha in distinct cell populations of different organs. *Faseb J*. **77**:271–273.
15. Loboda, A., Jozkowicz, A., and Dulak, J. (2010). HIF-1 and HIF-2 transcription factors--similar but not identical. *Molecules and Cells*, **29**: 435–42.
16. Gordan, J.D., Bertout, J.A., Hu, C.J., Diehl, J.A., Simon, M.C. (2007) HIF-2alpha promotes hypoxic cell proliferation by enhancing c-myc transcriptional activity. *Cancer Cell*. **11**: 335-47

17. Semenza, G.L. (2009) Regulation of cancer cell metabolism by hypoxia-inducible factor 1. *Semin Cancer Biol*. **19**:12–6.
18. Semenza, G.L. (2010) HIF-1: upstream and downstream of cancer metabolism. *Curr Opin Genet Devel*. **20**:51–6.
19. Semenza, G. L. (2013). HIF-1 mediates metabolic responses to intratumoral hypoxia and oncogenic mutations, *J. Clin Invest.* **123**: 3664-3671.
20. Maina, E.N., Morris, M.R., Zatyka, M., Raval, R.R., Banks, R.E., Richards, F.M., Johnson, C.M., Maher, E.R. (2005) Identification of novel VHL target genes and relationship to hypoxic response pathways. *Oncogene*. **24**: 4549-58.
21. Yuen, J.S., Cockman, M.E., Sullivan, M., Protheroe, A., Turner, G.D., Roberts, I.S., Pugh, C.W., Werner, H., Macaulay, V.M. (2007) The VHL tumor suppressor inhibits expression of the IGF1R and its loss induces IGF1R upregulation in human clear cell renal carcinoma. *Oncogene* **26**: 6499–508.
22. Shimobayashi, M., and Hall, M. N. (2014). Making new contacts: the mTOR network in metabolism and signalling crosstalk. *Nature Reviews. Molecular Cell Biology*, **15**: 155–62.
23. Cuperlovic-Culf, M., Ferguson, D. ,Culf, A., Morin, P. ,Touaibia, M. (2012) 1H NMR metabolomics analysis of glioblastoma subtypes: correlation between metabolomics and gene expression characteristics. *J Biol Chem,* **287** 20164-20174
24. Morin, P Jr., Ferguson, D., LeBlanc, L.M., Hebert, M., Pare, A., Jean-Francois, J., Surrette, M.E., Touaibia, M., Cuperlovic-Culf, M. (2013) NMR metabolomics analysis of the effects of 5-lipoxygenase inhibitors on metabolism in glioblasomas. *Jour Prot Res,* **12**: 2165-2176.
25. Lefort, N., Brown, A., Lloyd, V., Ouellette, R., Touaibia, M., Culf, A. S., & Cuperlovic-Culf, M. (2013). (1)H NMR metabolomics analysis of the effect of dichloroacetate and allopurinol on breast cancers. *J Pharm Biomed Anal.* **93**: 77-85.
26. Hwang, T., Shaka, A.J. (1995) Water suppression that works. Excitation sculpting using arbitrary waveforms and pulse field gradients. *J Magn Res A,* **112** 275-279.
27. Savorani, F., Tomasi, G., Engelsen, S.B. (2010) Icoshift: A versatile tool for the rapid alignment of 1D NMR spectra, *J Magn. Reson*. **202**: 190-202,
28. Tusher, V.G., Tibshirani, R. ,Chu G. (2001) Significance analysis of microarrays applied to the ionizing radiation response. *Proc Natl Acad Sci.* **98** 5116.
29. Maxwell, P.H., Wiesener, M.S., Chang, G.W., Clifford, S.C., Vaux, E.C., Cockman, M.E. et al.(1999). The tumor suppressorprotein VHL targets hypoxia-inducible factors for oxygen-dependent proteolysis.*Nature* **399**: 271–275.
30. Walker-Samuel, S., Ramasawmy, R., Torrealdea, F., Rega, M., Rajkumar,V., Johnson, S.P., Richardson, S., Gonçalves, M., Parkes, H.G., Arstad, E., Thomas, D.L., Pedley, R.B., Lythgoe, M.F., Golay, X. (2013) In vivo imaging of glucose uptake and metabolism in tumors. *Nat Med.* **19**:1067-72.
31. Kotze, H.L., Armitage, E.G., Sharkey, K.J., Allwood, J.W., Dunn, W.B., Williams, K.J., Goodacre, R. A (2013) novel untargeted metabolomics correlation-based network analysis incorporating human metabolic reconstructions. *BMC Syst Biol*. **23**: 7:107.
32. Jiang, W.G., Bryce, R.P., Horrobin DF: (1998) Essential fatty acids: molecular and cellular basis of their anti-cancer action and clinical implications. *Crit Rev Oncol Hematol*, **27**:179–209.
33. Knox, W.E., Tremblay, G.C., Spanier, B.B., Friedell, G.H. (1967) Glutaminase activities in normal and neoplastic tissues of the rat. *Cancer Res*, **27**:1456–1458.
34. Hu, H., Takano, N., Xiang, L., Gilkes, D.M., Luo, W., Semenza, G.L. (2014) Hypoxia-inducible factors enhance glutamate signaling in cancer cells. *Oncotarget*. **5:** 8853-68.
35. Long, J.S., Crighton, D., O'Prey, J., Mackay, G., Zheng, L., Palmer, T.M., Gottlieb, E., Ryan, K.M. (2013) Extracellular adenosine sensing-a metabolic cell death priming mechanism downstream of p53. *Mol Cell.* **50**: 394-406.
36. Antonioli, L., Blandizzi, C., Pacher, P., Haskó, G. (2013) Immunity, inflammation and cancer: a leading role for adenosine. *Nat Rev Cancer*. **13**: 842-57.

37. Nagaya, H., Gotoh, A., Kanno, T., Nishizaki, T. (2013) A3 adenosine receptor mediates apoptosis in in vitro RCC4-VHL human renal cancer cells by up-regulating AMID expression. *J Urol.* **189**: 321-328.
38. Biswas, S., Troy, H., Leek, R., Chung, Y.L., Li, J.L., Raval, R.R., Turley, H., Gatter, K., Pezzella, F., Griffiths, J.R., Stubbs, M., Harris, A.L. (2010) Effects of HIF-1alpha and HIF2alpha on Growth and Metabolism of Clear-Cell Renal Cell Carcinoma 786-0 Xenografts. *J Oncol*. **2010**:757908.
39. Sevcenco, S., Krssak, M., Javor, D., Ponhold, L., Kuehhas, F.E., Fajkovic, H., Haitel, A., Shariat, S.F., Baltzer, P.A. Diagnosis of renal tumors by in vivo proton magnetic resonance spectroscopy. (2014) *World J Urol*. Mar 9.

Figure Legends

FIGURE 1. ***VHL*** **transfection and** ***HIF-1α*** **and** ***HIF2α*** **silencing**. In RCC10 wild type both HIF-1α and HIF-2α are present. Transfection with *VHL* leads to deletion of either HIF-1α and HIF-2α. Individual silencing of *HIF-1α* and *HIF-2α* lead to expected changes in protein levels. A. Protein levels of HIF-1α and HIF-2α in RCC10 cells 72h post treatment. In RCC10 wild type (RCC10) both HIF-1α and HIF-2α are present. Transfection with *VHL* (RCC10/*VHL*) leads to deletion of both HIF-1α and HIF-2α. Individual silencing of *HIF-1α* and *HIF-2α* leads to expected changes in protein levels. B. Schematic outline of proteins expression of VHL, HIF-1α and HIF-2α in four groups of samples. C. Effect of *VHL* transfection and HIF-1α or HIF-2α silencing on the known targets of HIF proteins BNIP3 and VEGFA.

FIGURE 2. Principal component analysis (PCA) of metabolic data. PCA of intracellular (A, C) and extracellular (B, D) metabolite extracts showing profile difference between VHL- (blue) and VHL+ (red) cells after 48h (X) and 72h (O) in cell cultures. For comparison shown are results of PCA for spectra (Qualitative analysis – A and B) and metabolite concentrations (Quantitative analysis – C and D). An outlier in VHL-, 72h samples is marked with an *.

FIGURE 3. Correlation graph. Graph of Spearman correlations between metabolite concentrations at time points 48 and 72h Shown are correlations of over 0.85. A. Correlation network for VHL- (wild type RCC10) cells. B. Correlation network for VHL+ (transfected RCC10) cells.

FIGURE 4. Determination of major metabolic effects of VHL transfection. SAM analysis of RCC10 cells wild type (with mutated VHL and present HIF-1α and HIF-2α proteins) compared with *VHL* transfected RCC10 cells that have functional VHL and deleted HIF-1α and HIF-2α. Metabolic differences are caused by effects of VHL. Metabolic concentrations were first sample normalized followed by metabolite scaling across samples and shown are relative concentrations following this scaling. Also shown are fold changes for each significantly differentially concentrated metabolites (FC).

FIGURE 5. Determination of major metabolic effects of HIF-1α silencing. SAM analysis of RCC10 cells wild type (with mutated *VHL* and present HIF-1α and HIF-2α proteins compared with shHIF-1α treated RCC10 cells that have functional HIF-2α. Metabolic differences are caused by effects of HIF-1α. Metabolic concentrations were first sample normalized followed by metabolite scaling across samples and shown are relative concentrations following this scaling. Also shown are fold changes for each significantly differentially concentrated metabolites (FC).

FIGURE 6. Determination of major metabolic effects of HIF-2α silencing. SAM analysis of RCC10 cells wild type (with mutated *VHL* and present HIF-1α and HIF-2α proteins compared with shHIF-2α treated RCC10 cells that have functional HIF-1α. Metabolic differences are caused by effects of HIF-2α. Metabolic concentrations were first sample normalized followed by metabolite scaling across samples and shown are relative concentrations following this scaling. Also shown are fold changes for each significantly differentially concentrated metabolites (FC).

Supplementary Figures

FIGURE 1. Metabolite measurements for RCC10 cells. A. 1D 1H NMR spectra of RCC10 samples measured after 72h in culture following different treatments. Spectra from all replicates are superimposed. B. Relative concentrations of metabolites across all investigated samples in intracellular and extracellular medium. Concentrations of metabolites are scaled across samples and across metabolites leading to relative values shown.

FIGURE 2. Correlation coefficients calculation. Spearman correlation coefficients (absolute values) for intracellular metabolites. Shown are correlations from 0.5 to 1 obtained for VHL- cells (top triangle) and VHL+ cells (bottom triangle).

FIGURE 3. PCA of metabolic profiles (spectra) for different groups of RCC10 cells . A. comparison between RCC10 VHL- and RCC10 VHL+ cells; B. Comparison between RCC10/VHL- and cells with silenced HIF-1α or HIF-2α; C. Comparison between RCC10/VHL+ and cells with silenced HIF-1α or

HIF-2α. Difference between function of VHL, HIF-1α, HIF-2α in the groups compared here are shown above each plot (where for example +++ would describe cell with functional VHL, HIF-1α and HIF-2α proteins).

FIGURE 4. Subset of metabolic pathways with schematic representation of relative metabolite concentrations in VHL^- cells relative to VHL^+ shHIF1 and shHIF2 cells. Colored cells in mini tables show comparison of metabolite concentrations in VHL^- cells relative to VHL^+ shHIF1 and shHIF2 cells. Relative values in intracellular and extracellular samples are provided in top and bottom rows in tables respectively. Blue color indicates that concentration was higher in the first group in the comparison (i.e. VHL^-), red in the second group in sample comparison (VHL^+, shHIF1a and shHIF2). Included is a detailed Figure Legend providing information about the sample groups included in this analysis, color legend and the VHL, HIF-1α and HIF-2α expression in each compared group.

FIGURE 5. Subset of metabolic pathways with schematic representation of relative metabolite concentrations in in VHL^+ cells relative to VHL; shHIF1a and shHIF2 cells. Colored cells in mini tables show comparison of metabolite concentrations in VHL^+ cells relative to *VHL*; shHIF1a and shHIF2 cells. Relative values in intracellular and extracellular samples are provided in top and bottom rows in tables respectively. Blue color indicates that concentration was higher in the first group in the comparison (VHL^-, shHIF1a and shHIF2), red in the second group (VHL^+) in sample comparison. Included is detailed Figure Legend providing information about the sample groups included in this analysis, color legend and the VHL, HIF-1α and HIF-2α expression in each compared group.

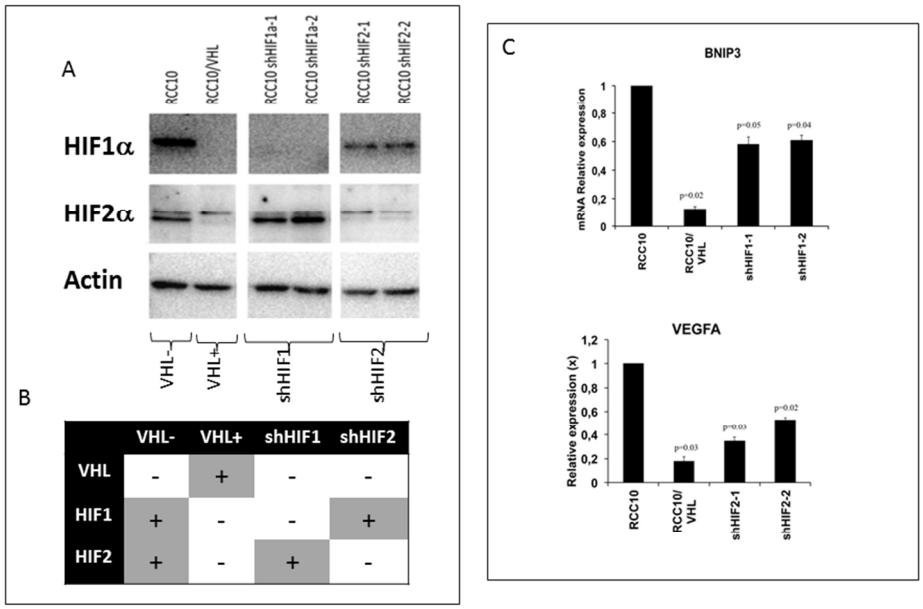

Figure 1.

FIGURE 1. VHL transfection and HIF-1α and HIF2α silencing. Protein levels of VHL, shHIF1 and shHIF2 RCC10 transfected cells. In RCC10 wild type both HIF-1α and HIF-2α are present. Transfection with VHL leads to deletion of either HIF-1α and HIF-2α. Individual silencing of HIF-1α and HIF-2α lead to expected changes in protein levels. A. Protein levels of HIF-1α and HIF2 in differently treated RCC10 cells 72h post treatment. In RCC10 wild type (RCC10) both HIF-1α and HIF-2α are present. Transfection with VHL (RCC10/VHL) leads to deletion of both HIF-1α and HIF-2α. Individual silencing of HIF-1α and HIF-2α leads to expected changes in protein levels. B. Schematic outline of proteins expression of VHL, HIF-1α and HIF-2α in four groups of samples. C. Effect of VHL transfection and HIF-1α or HIF-2α silencing on the known targets of HIF proteins BNIP3 and VEGFA.aaa
254x190mm (96 x 96 DPI)

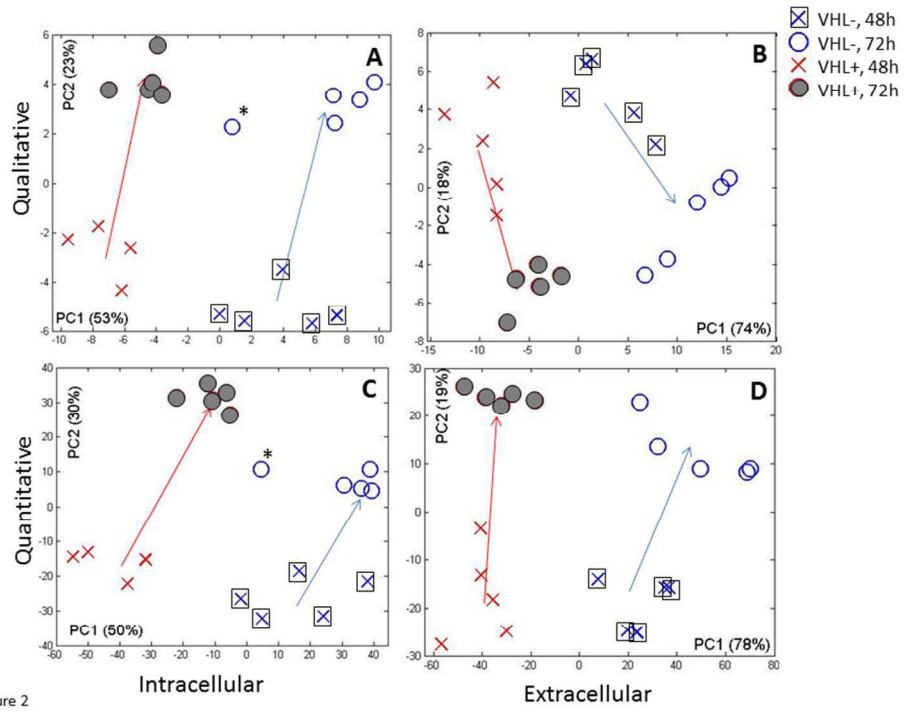

Figure 2

FIGURE 2. Principal component analysis (PCA) of metabolic data. Principal component analysis (PCA) of intracellular (A, C) and extracellular (B, D) metabolite extracts showing profile difference between VHL- (blue) and VHL+ (red) cells after 48h (X) and 72h (O) in cell cultures. For comparison shown are results of PCA for spectra (Qualitative analysis – A and B) and metabolite concentrations (Quantitative analysis – C and D). An outlier in VHL-, 72h samples is marked with an *.
254x190mm (96 x 96 DPI)

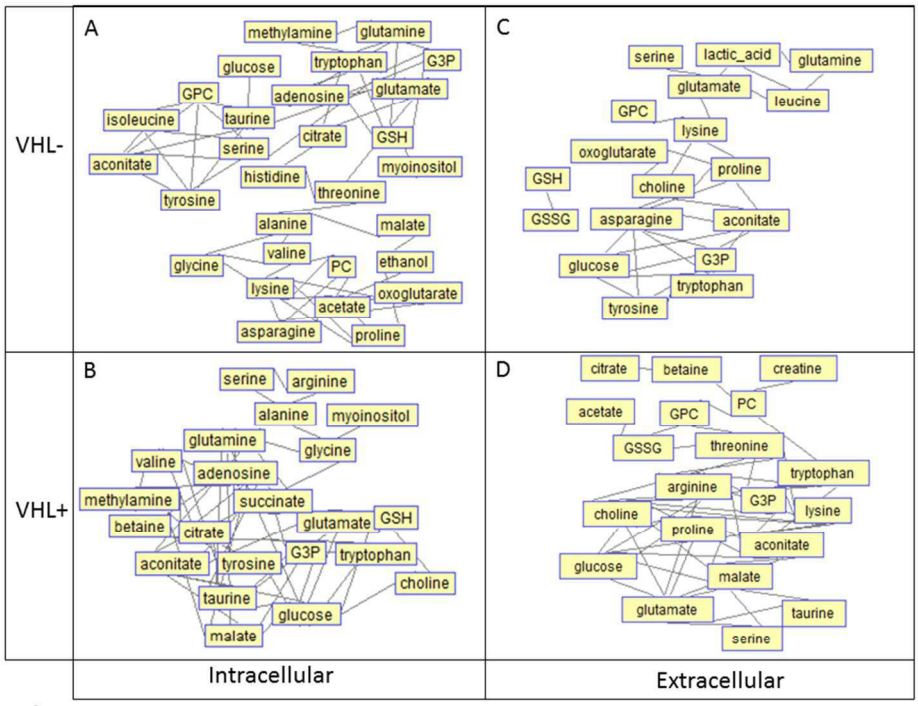

Figure 3

FIGURE 3. Correlation graph. Graph of Spearman correlations between metabolite concentrations at time points 48 and 72h Shown are correlations of over 0.85. A. Correlation network for VHL- (wild type RCC10) cells. B. Correlation network for VHL+ (transfected RCC10) cells.
254x190mm (96 x 96 DPI)

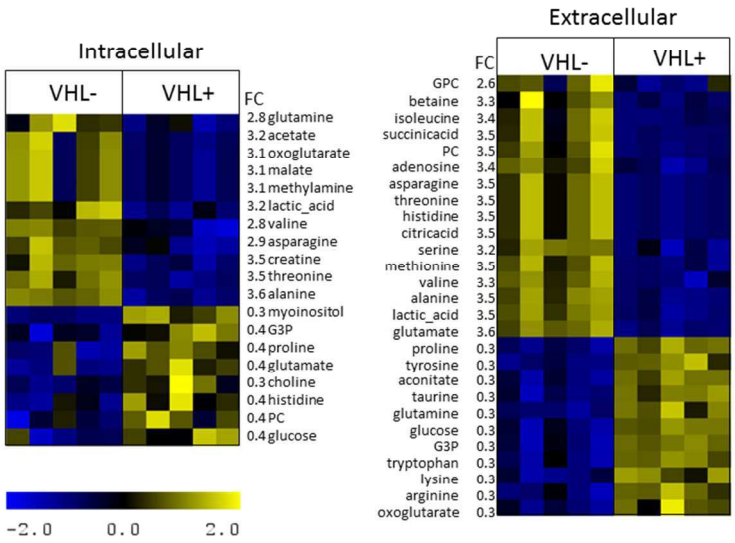

Figure 4

FIGURE 4. Determination of major metabolic effects of VHL transfection. SAM analysis of RCC10 cells wild type (with mutated VHL and present HIF-1α and HIF-2α proteins) compared with VHL transfected RCC10 cells that have functional VHL and deleted HIF-1α and HIF-2α. Metabolic differences are caused by effects of VHL. Metabolic concentrations were first sample normalized followed by metabolite scaling across samples and shown are relative concentrations following this scaling. Also shown are fold changes for each significantly differentially concentrated metabolites (FC).
254x190mm (96 x 96 DPI)

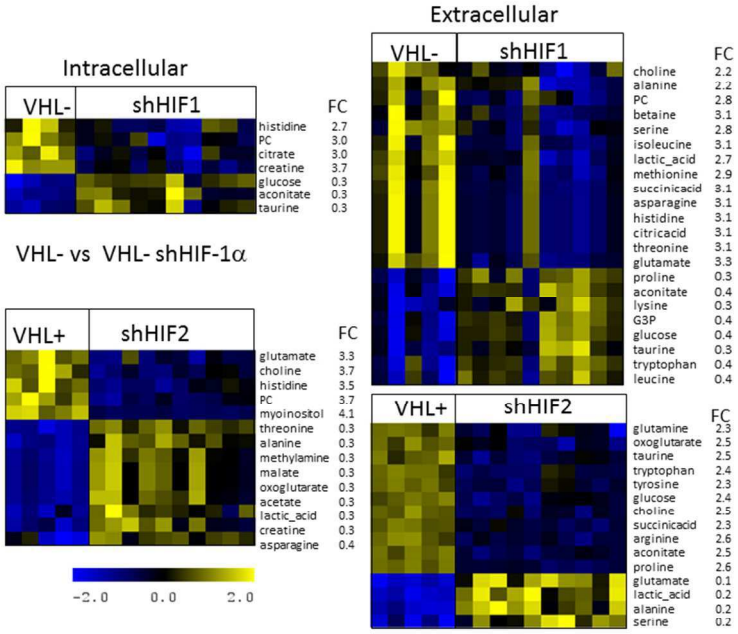

Figure 5

FIGURE 5. Determination of major metabolic effects of HIF-1α silencing. SAM analysis of RCC10 cells wild type (with mutated VHL and present HIF-1α and HIF-2α proteins compared with shHIF-1α treated RCC10 cells that have functional HIF-2α. Metabolic differences are caused by effects of HIF-1α. Metabolic concentrations were first sample normalized followed by metabolite scaling across samples and shown are relative concentrations following this scaling. Also shown are fold changes for each significantly differentially concentrated metabolites (FC). α
254x190mm (96 x 96 DPI)

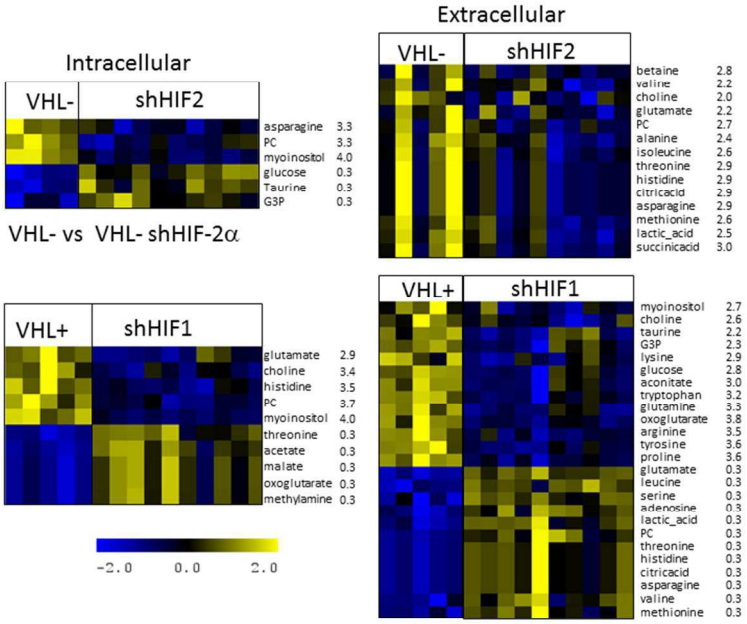

Figure 6

FIGURE 6. Determination of major metabolic effects of HIF-2α silencing. SAM analysis of RCC10 cells wild type (with mutated VHL and present HIF-1α and HIF-2α proteins compared with shHIF-2α treated RCC10 cells that have functional HIF-1α. Metabolic differences are caused by effects of HIF-2α. Metabolic concentrations were first sample normalized followed by metabolite scaling across samples and shown are relative concentrations following this scaling. Also shown are fold changes for each significantly differentially concentrated metabolites (FC). α
254x190mm (96 x 96 DPI)